Helium on planar and nanostructured alkali-metal surfaces

F. Ancilotto,[1] M. Barranco,[2] E. S. Hernández,[3] A. Hernando,[2] and M. Pi[2]
[1]*Dipartimento di Fisica "G. Galilei," Università di Padova, via Marzolo 8, I-35131 Padova, Italy and DEMOCRITOS National Simulation Center, I-34014 Trieste, Italy*
[2]*Departament d'Estructura i Constituents de la Matèria, Facultat de Física, and IN2UB, Universitat de Barcelona, 08028 Barcelona, Spain*
[3]*Departamento de Física, Facultad de Ciencias Exactas y Naturales, Universidad de Buenos Aires, Consejo Nacional de Investigaciones Científicas y Técnicas, RA-1428 Buenos Aires, Argentina*
(Received 12 December 2008; revised manuscript received 10 February 2009; published 19 March 2009)

We investigate the effects (on the wetting characteristics of helium below 3 K) of tailoring an alkali-metal surface by incorporating a regular array of nanoscopic indentations. We establish the prewetting line of helium on semi-infinite planar Cs up to 3 K in the frame of a finite-range temperature-dependent density-functional theory, and examine the modifications introduced in the isotherms when the substrate is covered with a periodic lattice of parabolic cavities. We show that, both for the planar and nanostructured surfaces, the unstable regions of the isotherms are stabilized by nucleation of drops and/or bubbles. Results corresponding to nonwettable Cs surfaces are compared with those obtained both for planar and nanopatterned Na substrates, where wetting at zero temperature is instead expected to occur, for a planar surface, preceded by a first-order prewetting transition.

DOI: 10.1103/PhysRevB.79.104514 PACS number(s): 68.08.Bc, 68.65.−k, 68.35.Np

I. INTRODUCTION

A cesiated surface exposed to helium vapor at tunable pressure and temperatures T below 4 K permits a beautiful realization of the first-order surface transition predicted by Cahn[1] and Ebner and Saam,[2] and is known as prewetting. Comprehensive reviews of this field that address the He-Cs system can be found in Refs. 3 and 4. For temperatures higher than a wetting one T_w and lower than a prewetting one T_{pw}, upon increase in the vapor pressure ^{4}He condenses on the substrate, forming a submonolayer film—metastable with respect to bulk helium—whose growth is abruptly interrupted by a finite jump in thickness at some value $\mu_{pw}(T)$ of the chemical potential, lower than the bulk liquid-vapor coexistence figure $\mu_0(T)$ at the given temperature. Further increase in the external pressure allows continuous growth of the stable thick film toward the bulk limit, and the curve $\Delta\mu(T)=\mu_{pw}(T)-\mu_0(T)$ for temperatures between T_w and T_{pw} is the prewetting line, with $\Delta\mu(T_w)=0$. The theoretical conjecture,[5] justified on thermodynamic arguments that helium would not wet weakly attractive substrates such as the heaviest alkali metals at zero temperature, was verified with the determination of the complete prewetting line for the system He-Cs,[6] establishing tentative values of 1.95 K for T_w and 2.5 K for T_{pw}.

Since these earlier experiments, subsequent measurements of helium adsorption isotherms and contact angle on Cs substrates indicated some dispersion in the above values, especially concerning T_w. Taking into account that these substrates are not samples of the pure metal but rather Cs films deposited on strong adsorbers such as gold, tungsten, or graphite, it has been argued that the wetting behavior of helium is heavily dependent on the process of construction of the film and/or its thickness. Reported values of T_w range roughly between 1.5 K in Ref. 7 and 2.2 K in Ref. 8; furthermore, an analysis of wetting temperatures detected on Cs substrates of increasing thickness[7] suggests a limit of around 2.3 K for the semi-infinite material. Attempts to measure the contact angle $\theta(T)$ and to extract the wetting temperature by extrapolation to vanishing θ, presented in Refs. 8–11, locate T_w between 1.75 and 2.179 K,[8] and it has become common practice to assign a value of T_w to each specific Cs substrate,[8,12] in view of the fact that varying the width of deposited Cs is a convenient strategy to tune the ^{4}He-Cs interaction and thus the wetting diagram of the system.[7] Some uncertainties may also obscure the established value of T_{pw} around 2.5 K,[13] as the experimental isotherms above that temperature still exhibit a somewhat visible jump, as shown for instance in Ref. 6 for the isotherm at 2.7 K.

In addition to the above mentioned results, it is agreed that surface roughness is an important source of variations in the wetting diagram for substrates built out of the same material under different mechanisms. Moreover, abundant experimental research concentrates on memory effects and hysteresis in the dynamics and shape of the contact line of liquid-helium flooding a Cs substrate,[9–12] showing that the presence of microcavities is the key for the change in the finite contact angle of an advancing front into a vanishing angle for the receding contact line. The existence of hysteresis represents an extra complication in any determination of T_w and the prewetting line. These observations converge toward the convenience of establishing a theoretical reference, namely, the prewetting line of helium on an ideal Cs substrate such as the homogeneous semi-infinite solid, which offers to the atoms in the vapor the most trustworthy adsorbing potential established up to date.[14]

More recently, the existence of natural and manufactured nanopores[15,16] on the one side, and, on the other, the possibility of growing surfaces structured within the nanoscale, triggered experimental and theoretical lines of research, oriented toward pore filling and wetting of nanopatterned substrates by classical fluids.[16–18] The condensation of helium in

nanopores at zero temperature has been analyzed using variational Jastrow-Feenberg,[19] variational Monte Carlo,[20] and mean field[21,22] techniques; in particular, we have proven that finite-range density-functional (FRDF) theory is a powerful instrument in detecting multiple equilibrium states and trace hysteretic loops in the road toward capillary condensation of helium in weakly adsorbing pores.[22] On the other hand, finite temperature FRDF is also adequate in examining aspects of wetting properties of helium on Cs, such as the contact angle[23,24] and the wetting temperature of the semi-infinite metal.[25] Other applications of T-dependent density functionals in describing liquid-gas coexistence, and interfacial properties of superfluid and normal ^{4}He validate this approach.[26]

In view of all considerations above, in this work we aim at examining, in the frame of finite temperature-FRDF theory, the characteristics of the prewetting line and prewetting isotherms of the ^{4}He-Cs system, and their modifications in the presence of a Cs surface patterned with an array of parabolic finite nanocavities. Such a configuration is inspired on a silica substrate recently created and exposed to a hydrocarbon vapor,[27] bringing into evidence a strong influence of geometrical and finite-size effects in the dependence of $\Delta\mu$ upon the amount of adsorbed material. To fulfill our purpose, we accomplish a necessary preliminary step: employing the T-dependent FRDF of Ref. 25, we carry on the theoretical construction of the coexistence phase diagram and prewetting line of ^{4}He on homogeneous semi-infinite Cs up to 3 K. The addition of cavities, which breaks translational invariance, provides a collection of nucleation sites where finite systems such as drops and bubbles may locate, giving rise to important deviations of the isotherms with respect to those for the flat surface. Finally, we compare all results with corresponding ones for the system ^{4}He on Na substrates, which are wetted at zero temperature.

This paper is organized as follows. In Sec. II we recall the essentials of finite temperature FRDF and describe our numerical procedure. In Sec. III we present the results for planar and nanostructured Cs substrates, and in Sec. IV, for planar and nanostructured Na substrates. The outcome of this work is summarized in Sec. V.

II. THEORY AND NUMERICAL PROCEDURE

Density-functional theories at finite temperatures[28] involve minimization, with respect to an inhomogeneous density $\rho(\mathbf{r})$, of a thermodynamic grand potential

$$\Omega(\mu,T) \equiv F(T) - \mu(T)N = \int d\mathbf{r}\{f[\rho(\mathbf{r}),T] - \mu\rho(\mathbf{r})\}, \quad (1)$$

with $F(T)$ as the total free energy in terms of a density kernel $f[\rho,T]$, parametrized as indicated, e.g., in Refs. 25 and 26, N as the mean number of helium atoms in the system, and $\mu(T)$ as their chemical potential. This is a grand canonical procedure where, given the expectation value of the atom number, one solves the Euler-Lagrange (EL) equation corresponding to the functional variation $\delta\Omega=0$, carried with respect to the local density; this yields the integrodifferential nonlinear equation $\delta f/\delta\rho=\mu$. We have employed the FRDF of Ref. 25; details of this type of calculations can be found in, e.g., Refs. 29 and 30 and references cited therein, so we just mention here the essentials of the method as applied to this particular problem.

We first cast the EL equation into a Schrödinger-type equation.[31] To this end, we write the free-energy density as $f \equiv \frac{\hbar^2}{2m_{\mathrm{He}}}|\nabla\Psi|^2 + \mathcal{F}$, where $\Psi(\mathbf{r}) \equiv \sqrt{\rho(\mathbf{r})}$. The EL equation then reads

$$-\frac{\hbar^2}{2m_{\mathrm{He}}}\Delta\Psi + \left\{\frac{\delta\mathcal{F}}{\delta\rho} + V_{X\text{–He}}\right\}\Psi = \mu\Psi, \quad (2)$$

where $V_{X\text{–He}}$ is He atom-substrate potential. The differential operators in Eq. (2) have been discretized using 13-point formulas for the derivatives, and the resulting equation has been solved employing an imaginary time method.[31,32] The stability of the calculations has been checked against reasonable changes in the value of the spatial steps.

Throughout this work we have used Cartesian coordinates. A cornerstone in our method of solving the EL equation is the use of fast Fourier transformation techniques (FFT) (Ref. 33) to efficiently compute the convolution integrals entering the definition of $\mathcal{F}(\rho)$. While this is not crucial for one-dimensional (1D) problems, it turns out to be important when addressing two-dimensional (2D) and three-dimensional (3D) situations. Inherent to the use of FFT is to impose periodic boundary conditions inside a unit cell. This is irrelevant if the system under study is finite, as a helium drop, whose density goes to zero at large enough distances.

For planar surfaces, $V_{X\text{–He}}$ has been taken from Ref. 14. We compute density profiles in a unit cell allowing a height $z_{\max}$ large enough to host homogeneous vapor, characterized by a density ρ_{gas}, on top of the adsorbed film. To be more specific, within the unit cell we have accommodated two planar surface substrates perpendicular to the relevant z direction and have used $N_z=2048$ points. This corresponds to $N_x \times N_y \times N_z = 1 \times 1 \times 2048$ points for the FFT. Each planar substrate is located 55 Å inside the cell boundaries. Since our mesh size is $\Delta z=0.4$ Å, this leaves about 709 Å between the planar surfaces to accommodate the helium gas and the adsorbed fluid. In the course of the imaginary time minimization, the whole system has been forced to be symmetric with respect to the plane bisecting the unit cell between the two planar substrates. Consequently, the physical system is represented by the contents of half the unit cell. In this way, on the one hand we guarantee that the influence of surrounding cells is negligible, and on the other, we leave enough room inside the cell so that the filling vapor does indeed correspond to the equilibrium helium gas at the given T and μ.

In practice, we have proceeded in a different but equivalent way by fixing a temperature T and number of He atoms N. The self-consistent solution of Eq. (2) determines $\rho(\mathbf{r})$ and μ. In this case, the consistency test consists in checking that the helium vapor density—helium density in the middle of the unit cell at ~355 Å from the planar adsorber—coincides with the gas density ρ_{gas} at the given T and the *calculated* μ.

Figure 1 displays the density profile corresponding to helium on a planar Cs substrate at $T=2.3$ K. It corresponds to

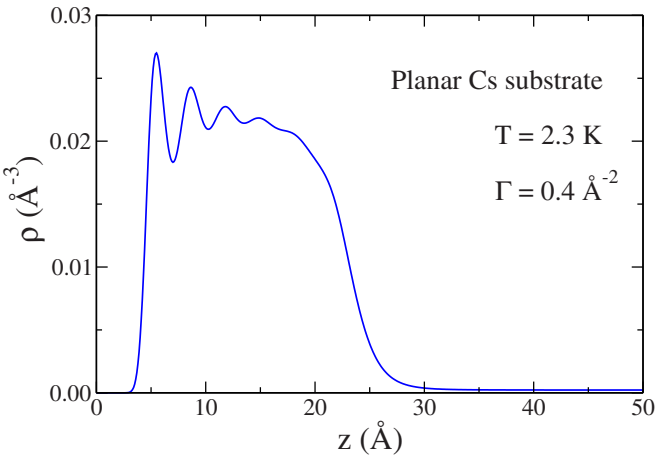

FIG. 1. (Color online) Density profile corresponding to helium on Cs at $T=2.3$ K and $\Gamma=0.40$ Å^{-2}. The Cs substrate is located at $z=0$.

a coverage $\Gamma=0.4008$ Å^{-2}, established as defined below. Solving Eq. (2) we have determined the chemical potential $\mu=-7.5786$ K and vapor density at 355 Å from the Cs surface, $\rho_v=2.218\,84\times10^{-4}$ Å^{-3}. The helium gas density, obtained from the bulk equation of state for the above temperature and chemical potential, is $\rho_{\rm gas}=2.218\,86\times10^{-4}$ Å^{-3}. This is the typical excellent agreement between ρ_v and $\rho_{\rm gas}$ found in our calculations, showing the adequacy of the selected unit cell. Knowledge of $\rho(\mathbf{r})$ and μ at fixed T permits the construction of adsorption isotherms $\mu(\Gamma,T)$, where Γ is the coverage

$$\Gamma=\frac{1}{\mathcal{S}}\int d\mathbf{r}\ \mathrm{Max}\{0,[\rho(\mathbf{r})-\rho_{\rm gas}]\},\tag{3}$$

i.e., adsorbed fluid per unit area, and where in practice $\mathcal{S}$ is the surface of the unit cell in the (x,y) plane, and $\rho(\mathbf{r})$ is the helium density within the cell.

To address nanostructured surfaces, one has to obtain first an accurate surface-He atom interaction potential $V_{X\text{–He}}$. This is a nontrivial task that strictly requires a first-principles calculation for every particular geometries, and it is beyond current state-of-the-art approaches. Recently, we have presented a method to generate adsorption potentials starting from a known adsorption field for a planar surface.[34] It assumes a continuous distribution of sources, thus neglecting any possible crystal structure of the adsorbing surface. In cases where the physical effects of such structure can be safely neglected, as for alkali-metal surfaces interacting with liquid helium, it provides a good adsorption potential for nonplanar geometries.[22]

We have considered an alkali planar surface hosting a periodic array of parabolic nanocavities of height $h=35$ Å and outer radius $R=25$ Å lying on the (x,y) plane. This geometry is inspired on substrates studied in Ref. 27 and suggestions made in Ref. 11. We have considered one such nanocavity per unit cell. In this case, the calculation is fully 3D and the size of the unit cell has obvious computational limitations. The nanostructured substrate is located inside the boundaries of a $N_x\times N_y\times N_z=128\times128\times256$ cell, and the

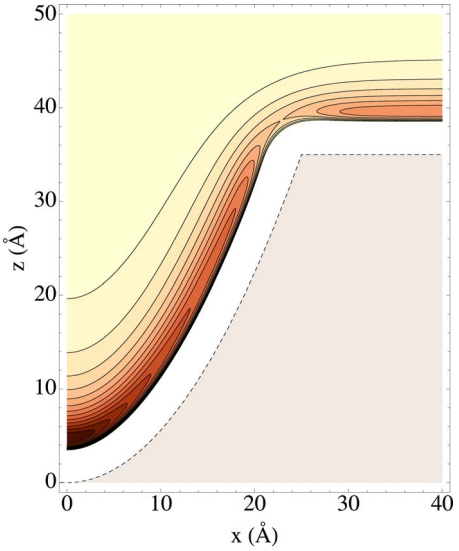

FIG. 2. (Color online) Isopotential lines for $y=0$ and $x\geq0$ of the adsorption potential created by a parabolic cavity of 35 Å height and outer radius $R=25$ Å in a planar Cs surface (dashed line). The isopotential lines have been drawn from 0 to −14 K in −1 K steps. The line closer to the Cs substrate corresponds to the repulsive core at 0 K, and the outermost line to −1 K. The absolute minimum is −14.05 K, near the vertex of the paraboloid—note that the darker the region, the more attractive the potential. It is worth seeing the heliophobic ring around the top of the cavity, where the minimum of the potential is just −3.99 K instead of the −6.93 K value that corresponds to the absolute minimum of the planar Cs surface.

size steps are $\Delta x=\Delta y=0.9$ Å, and $\Delta z=0.6$ Å. This corresponds to a fairly structured adsorbing surface with $\sim7.5\times10^{11}$ cavities/cm^2 and an aspect ratio $\pi R^2/\mathcal{S}\sim0.148$.

Figure 2 displays the contour plot of the adsorption potential created by such a structured Cs surface. It is worthwhile recalling that the potential is axially symmetric around the cavity but not near the unit-cell boundary in the (x,y) plane. This will influence the way in which helium condenses on the surface, yielding different patch geometries whose relative stability will depend on the coverage and will cause the appearance of hysteretic cycles.

For computational limitations, we cannot proceed as for planar surfaces, for which we have placed two structured surfaces inside the unit cell, since this would require twice as much points in the z direction, N_z. If we use a single surface, near $z_{\rm max}\sim154$ Å in our case, the helium gas in the unit cell feels the repulsion from the bulk alkali in the cells stacked on the top and ρ_v goes to zero as $z\to z_{\rm max}$. The effect of this spurious inhomogeneity on the results is negligible because ρ_v is small even at the largest temperature in our calculations (recall, e.g., the value of ρ_v shown in Fig. 1). We have checked that, at distances far enough from the substrate, the variational helium density profile $\rho(\mathbf{r})$ is flat and its value is sensibly the same as the corresponding $\rho_{\rm gas}$. This is so because there are about 154 Å on top of the adsorbing surface to accommodate the gas; consequently, the vapor inhomogeneity does not influence the numerical results. For instance, solving Eq. (2) in the case of a structured Cs surface at $T=2.3$ K and $\Gamma=0.2667$ Å^{-2}, we have found $\mu=-7.7146$ K

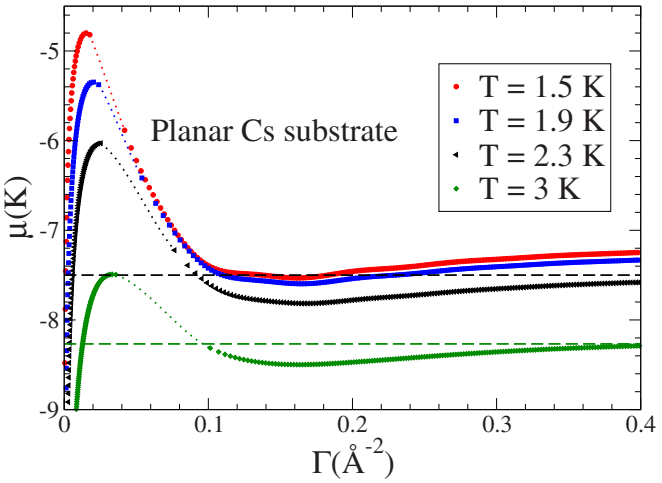

FIG. 3. (Color online) Isotherms for helium on planar Cs substrates at $T=1.5$, 1.9, 2.3, and 3 K. The horizontal lines indicate the chemical potentials corresponding to the two Maxwell constructions for the isotherms with $T>T_w\sim 2.05$ K.

and a vapor density $\rho_v=2.086\times 10^{-4}$ Å^{-3}, whereas for this temperature and chemical potential, one has $\rho_{gas}=2.084\times 10^{-4}$ Å^{-3}, in very good agreement with ρ_v. The coverage Γ is defined as before and represents an average value within the cell or, equivalently, on the adsorbing surface. Examples of the equilibrium configurations will be presented in the following sections.

III. RESULTS FOR CS SUBSTRATES

A. ^{4}He on planar Cs

1. Homogeneous film

We have calculated several isotherms around $T=2$ K up to a fairly large coverage, $\Gamma\sim 2$ Å^{-2}. This allows us to carry out Maxwell constructions to determine the wetting temperature. We display in Fig. 3 typical isotherms for $T=1.5$, 1.9, 2.3, and 3 K up to $\Gamma=0.4$ Å^{-2}. For the cases where a Maxwell construction is possible, i.e., above the wetting temperature, we have drawn a horizontal line representing the chemical potential at phase coexistence. It intersects the corresponding isotherm at a lower (Γ_t) and higher (Γ_T) coverage whose corresponding configurations are in equilibrium along the prewetting line (see the discussion below). For each isotherm, we have computed both the adsorption and desorption branches—i.e., increasing and decreasing the total number of particles in the unit cell—and have checked that they coincide, revealing the absence of hysteretic loops.

The isotherms display a gap inside the unstable ($d\mu/d\Gamma<0$) region, where we have been unable to find a solution to the EL equation. To connect the two calculated pieces depicted with symbols, we have employed a cubic spline, whose result for the gap is represented by dotted lines in Fig. 3. It can be seen that the behavior of the isotherms as a function of Γ is very smooth. Rather than a shortcoming of the calculation, the appearance of this gap reflects a physical fact. It appears that, as the coverage increases along a given isotherm, the vapor on top of the adsorber surface eventually reaches the unstable (spinodal) region where the helium gas is no longer mechanically stable. This leads to a sudden condensation on the substrate and a decrease in the vapor density, bringing its value to the range of allowed—stable—vapor densities at the given T. We have confirmed this by calculating the equation of state of *homogeneous* liquid helium using the finite-T FRDF and determining the spinodal region as in Ref. 26. In short, one can only find solutions to Eq. (2) that asymptotically correspond to a stable helium vapor. The presence of a gap in the isotherms as a function of coverage has been also encountered in Monte Carlo calculations carried in the interior of a spherical cavity filled with a Lennard-Jones fluid.[35] These authors have used the gauge cell Monte Carlo method to determine a continuous path of equilibrium, yet unstable, configurations in order to fill the gap.[36]

With the series of isotherms completed in this way, we have performed Maxwell constructions to determine T_w. In particular, for the isotherms displayed in Fig. 3, we have found that the area between the chemical potential of bulk liquid helium at the corresponding T and the associated isotherm is negative for $T=3$ and 2.3 K, positive for $T=1.5$ and 1.8 K, and zero when $T=2.05$ K (wetting temperature). This calculation of T_w, based on an explicit and most complete determination of the isotherms, yields a figure compatible with the set of experimentally established values. It agrees well with that in Ref. 25 derived from the same FRDF by computing the interfacial tensions between each pair of coexisting phases—liquid, solid, and vapor—which allows getting of the temperature at which the contact angle, obtained through the Young equation, becomes zero.

For temperatures above T_w, we can look for two films with the *same* chemical potential μ such that, if placed next to each other on the planar substrate, would coexist with a common helium vapor. To determine these configurations, we carry on Maxwell constructions that allow us to locate the prewetting jump between coexisting thin (Γ_t) and thick (Γ_T) films, and the corresponding deviation $\Delta\mu(T)$ difference between the chemical potential determined from the Maxwell construction and the bulk helium chemical potential at the given T. Two such Maxwell constructions have been presented in Fig. 3. We have plotted in Fig. 4 the locus of the thin-film–thick-film coexistence plateaus along the isotherms in the (Γ,T) plane, and the prewetting line (inset). Unfortunately, the prewetting temperature cannot be reached with the current T-dependent FRDF since the parameters have not been provided for temperatures above 3 K.

The jumps in film thickness depicted in Fig. 4 amount to several layers in the whole calculated range. In Fig. 5 we plot the density profiles of the coexisting thin and thick films at $T=2.3$ K. From these profiles we extract widths at half height of nearly 4 and 50 Å for the low and high coverages, respectively, which for the corresponding saturation density represent a thin film slightly above one monolayer, and a thick one with around 14 helium layers. On the experimental side, photoelectron tunneling measurements[37] indicate that below T_w and far from bulk coexistence the helium system is dilute with a coverage of less than one layer. Ellipsometric measurements of film thickness of helium on evaporated Cs with submonolayer resolution[38] indicate that, at $T=2.34$ K,

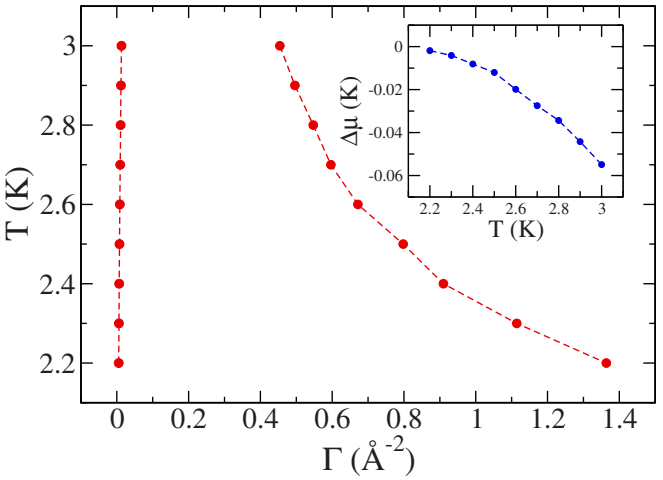

FIG. 4. (Color online) Thin-film–thick-film coexistence region for helium on an ideal planar Cs substrate below $T=3$ K. The inset shows the prewetting line $\Delta\mu$(K) as a function of T(K). The dashed lines are only a guide to the eye.

the thin film is around two layers wide and the prewetting jump could be estimated as 12–15 layers. The present results are then consistent with such experimental measurements, considering the difficulties inherent to addressing submonolayer films with photoelectrons because of the image potential.[39]

2. Cavitation and nucleation on planar Cs substrates

In the case of classical systems, it has been shown[40] that, since the thin film can exist above T_w in a metastable state, the decay of this state starts with the nucleation and growth of supercritical drops on the wall. Complementarily, it has been proposed[41] that, given a stable film that uniformly wets a substrate, dewetting occurs by the nucleation and spreading of dry patches on the film. On energetic grounds, it is well established that cohesion among absorbate atoms is the driving force of instabilities and dewetting, whereas adhesion to the substrate through van der Waals forces is the main agent

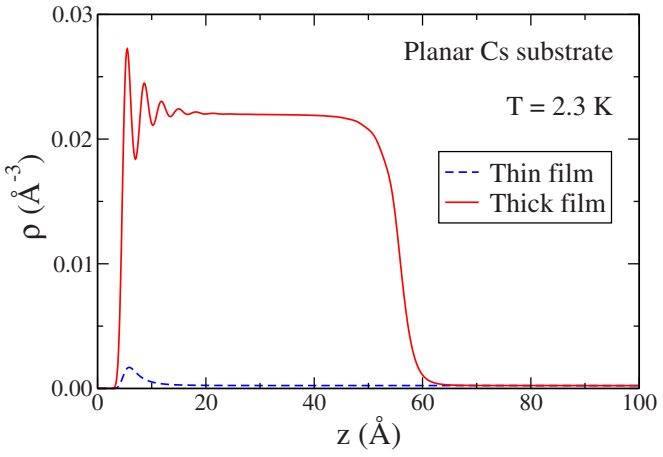

FIG. 5. (Color online) Density profiles of the thin and thick helium films that coexist at $T=2.3$ K. The Cs substrate is located at $z=0$.

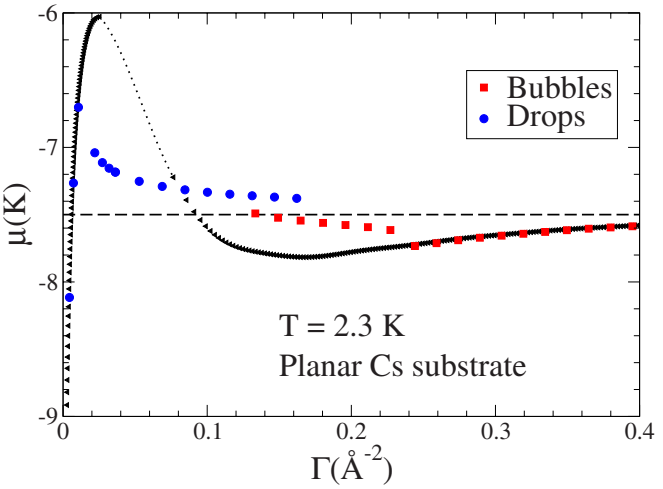

FIG. 6. (Color online) Isotherm for helium on planar Cs substrate for $T=2.3$ K (triangles and dotted line). The dashed horizontal line represents the chemical potential at which thin and thick films with coverages $\Gamma_t=5.9\times10^{-3}$ Å^{-2} and $\Gamma_T=1.11$ Å^{-2} (not shown) are in equilibrium with a common helium vapor. Circles (squares) represent drop (bubble) configurations found in the adsorption (desorption) process, except for configurations lying on the planar surface isotherm, which have been found to be uniform. A hysteretic loop is clearly visible.

of stability and wetting. A series of subsequent experiments for classical systems demonstrate nucleated dewetting and the observations can be well described by a simple classical nucleation model.[42] Moreover, coexisting thin and thick film domains have been detected in experiments involving water on mica.[42,43]

The prewetting jump may proceed by nucleating patches of the thick film (drops) within the thin film, as the average Γ increases, or by nucleating patches of the thin film (bubbles) within the thick film, as the average Γ decreases. We show in Fig. 6 the $T=2.3$ K isotherm displaying the regions where bubbles and drops have been found starting the imaginary time evolution from a configuration with the sought shape; this 3D calculation has been carried out as outlined in Sec. II.

We have also done some preliminary calculations showing that, above T_w, our numerical procedure is able to address the coexistence of a thin film with a thick one on a planar Cs substrate in equilibrium with a common helium vapor. Viewed as a first-order transition where a planar Cs surface with initial coverage Γ_t evolves toward a final coverage Γ_T at fixed T, or the other way around, the prewetting transition would occur by displacing the line that separates the coexisting regions with respective coverages Γ_t and Γ_T on the alkali surface, in a similar way as the liquid-gas transition in liquid helium takes place at equilibrium. We point out that nucleation and cavitation in liquid helium have been reviewed in Refs. 44 and 45.

As shown in Fig. 6, a remarkable aspect of the suppression of translational invariance due to the appearance of either bubbles or drops is the ability of the homogeneous surface to overcome mechanical instabilities by nucleating finite configurations. Indeed, opposite to the case reported in Fig. 3, we can find solutions of the EL equation in the whole

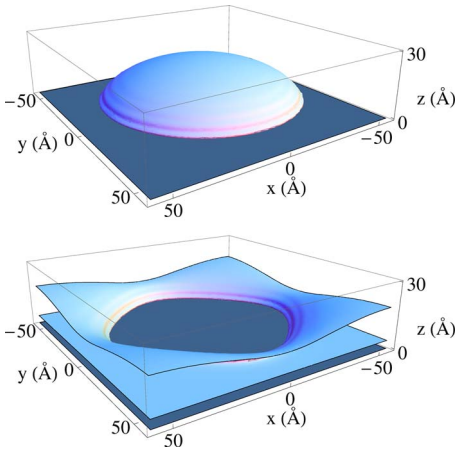

FIG. 7. (Color online) Bubble (bottom) and droplet (top) equilibrium configurations at $T=2.3$ K for helium on the planar Cs substrate corresponding to the points displayed in Fig. 6 at $\Gamma \sim 0.15$ Å^{-2}. The figure displays the isodensity surfaces corresponding to $\rho=0.011$ Å^{-3}, i.e., half the bulk liquid density at $T=0$ K. The dark area represents the Cs planar surface. Notice that, in the bottom panel, liquid helium fills the region between the two sheets representing the $\rho=0.011$ Å^{-3} isodensity surface. The stratification of the density due to the effect of the Cs surface is clearly visible at the edge of both drop and bubble configurations.

range of atom numbers, i.e., no gaps in coverage appear in the computed isotherm. We note that the presence of such finite configurations is limited to within the region where the Maxwell construction can be carried out, whereas the stable equilibrium configuration for low and large coverages is always the homogeneous film. For coverages close to Γ_t (Γ_T), the finite objects are small isolate drops (bubbles). For intermediate Γ values, bubbles and drops grow in size, and in that region the aspect of the isotherm unavoidably depends on the size of the unit cell. Likely, other finite-size structures, some perhaps more stable than drops and bubbles, might exist in that region; slabs are one such possibility, compatible with the imposed periodic boundary conditions. The appearance of these configurations in 3D fluids is well known, see, e.g., Ref. 46 for the very interesting case of the equation of state of hot dense stellar matter.

Associated with the existence of these finite configurations is the presence of hysteretic loops. Figure 6 shows one such loop when bubbles and drops are allowed to nucleate on the Cs substrate. Figure 7 shows the bubble and droplet equilibrium configurations corresponding to the calculated points displayed in Fig. 6 at $\Gamma \sim 0.15$ Å^{-2}. It is worth seeing that while the drop configuration is fairly circularly symmetric, the shape of the bubble is far from that symmetry. The reason is that this coverage is rather close to Γ_t and far from Γ_T in the coexistence region at $T=2.3$ K, see Fig. 4. Hence, the drop is fairly isolated whereas the bubble is not. Moreover, the analysis of the thermodynamic grand potential shows that the drops are the most stable configurations, however with a small energetic gain.

These calculations indicate that a thick helium film on planar Cs desorbs mostly by creation of holes. Such a behavior has been noted in the literature through numerous experiments and theoretical accounts, and it has been pointed out as well the possibility of an alternative mechanism of dewetting, namely, the nucleation of drops that stabilize on top of the thin film.[47] We want to mention that the coexistence of a thin and a thick helium film on Cs with a common vapor above T_w has not been ever observed experimentally because, as pointed out in Ref. 3, the thick film is likely nucleated from adjoint surfaces. Nevertheless, in the ideal situation discussed here of an unlimited planar Cs surface, coexistence should appear on the basis of solid thermodynamic arguments. This opens the possibility of extracting the line tension of helium on an ideal planar Cs surface as a function of T from 3D FRDF calculations, extending in this way prior work,[48] and address in detail nucleation and cavitation on the same substrate.[3] We plan to address these issues in a forthcoming work.

B. ^{4}He on nanostructured Cs

We now investigate the modification of the previous results by changing the planar substrate into the regular array of parabolic nanocavities described in Sec. II. This breaks planar translational invariance and introduces heliophilic adsorbing sites of enhanced strength that behave as nucleation seeds, such as the bottom of the parabolic cavity, as well as desorbing sites of reduced strength that behave as heliophobic sites, such as the annulus around the top of the cavity, see Fig. 2. One should then expect the spontaneous formation of inhomogeneities such as drops and bubbles in a wide interval of coverages. Eventually, for large enough coverages the structured Cs surface is fully covered by helium and the isotherm should resemble that of a planar surface. Notice that, where the parabolic nanocavities transformed into parabolic nanohills, the heliophilic and heliophobic sites would be reversed and, at low coverages, the annulus around the hill would nucleate quasi-one-dimensional liquid ^{4}He rings.

As the smooth surface becomes irregular, differences in wettability of flat and curved regions can be expected to accelerate dewetting since atoms in the thick film have the possibility of migrating toward the most heliophilic sites, leaving dry patches on the substrate.[43,49,50] In particular, 3D simulations and experiments performed on classical systems indicate that substrate heterogeneities can destabilize thick stable films;[50] dramatically enough, it has been shown that surface irregularities in the atomic scale can change a wetting system into a nonwetting system.[51] In our case, Fig. 8 shows how the isotherm at $T=2.3$ K is modified by the presence of the parabolic cavity. Either finite or extended configurations are found to be stable for all coverages, with drops possessing the lowest grand potential. Compared with the planar surface isotherm, the rightward shift of the structured surface isotherm is due to condensation of droplets at the bottom of the cavity at low coverages. When the coverage is large enough, e.g., $\Gamma \sim 0.35$ Å^{-2}, the nanopatterned isotherm is built from equilibrium configurations where filled cavities are covered with a nearly uniform helium film. Consequently, the nanopatterned isotherm merges with the planar one.

The wetting sequence illustrated in Fig. 8 with circles starts at low coverages by condensation of drops at the he-

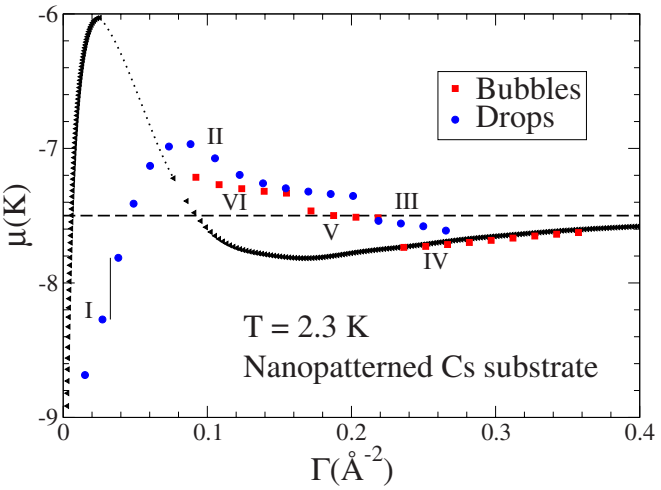

FIG. 8. (Color online) $T=2.3$ K isotherm for helium on the nanopatterned Cs substrate described in the text. The result for the planar surface is also shown (triangles and dotted line), and the dashed horizontal line has the same meaning as in Fig. 6. Circles (squares) represent finite configurations found in the adsorption (desorption) process, except for configurations lying on the planar surface isotherm, which have been found to be nearly uniform on top of the filled cavity. The roman numerals I–VI indicate the regions where different types of finite configurations have been found in the calculation, and the thin vertical line separates the regions of types I and II. Hysteretic loops are clearly visible.

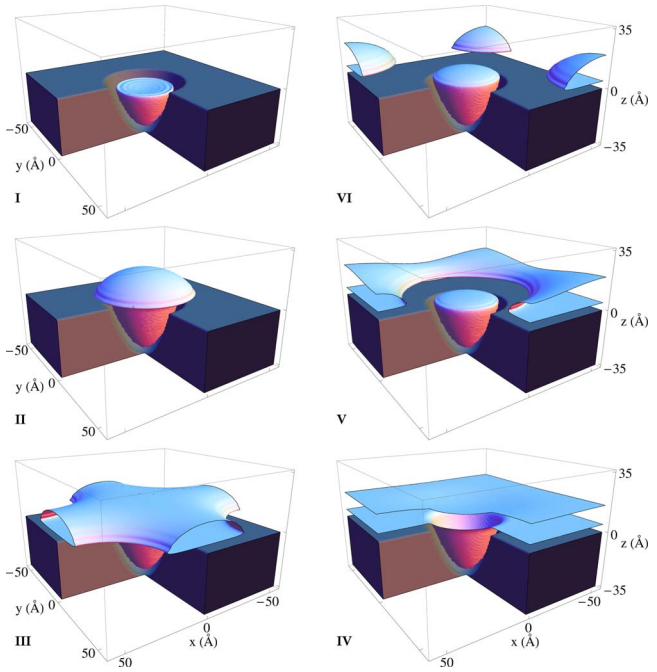

FIG. 9. (Color online) Counterclockwise, starting from the top left corner, the panels represent some illustrative equilibrium configurations for helium on the nanopatterned Cs substrate corresponding to regions I–VI in Fig. 8. Chosen coverages: region I, $\Gamma=2.73\times10^{-2}$ Å^{-2}; region II, $\Gamma=0.105$ Å^{-2}; region III, $\Gamma=0.219$ Å^{-2}; region IV, $\Gamma=0.267$ Å^{-2}; region V, $\Gamma=0.189$ Å^{-2}; region VI, $\Gamma=0.108$ Å^{-2}. The panels display the isodensity surfaces for $\rho=0.011$ Å^{-3}, i.e., half the bulk liquid density at $T=0$ K. The dark area represents the Cs planar surface. The stratification of the density due to the effect of the structured Cs surface is clearly visible at the edge of finite configurations.

liophilic bottom of the cavity, which acts as a nucleation site. This region is denoted by I in that figure. The cavity becomes filled at $\Gamma\sim3.3\times10^{-2}$ Å^{-2} and from this coverage on, the condensed droplet spreads outside. This corresponds to region II in the figure. Eventually, the drops are so large that only some spots at the corners of the unit cell in the (x,y) plane are relatively dry (region III); finally, the whole surface is covered by a thick helium film and from this point on, one recovers the planar surface isotherm (region IV). The dewetting sequence indicated by squares starts from the latter kind of configurations (region IV) and, as coverage decreases, helium is expelled from the heliophobic ring around the cavity edge, remaining its interior filled with helium (region V). Finally, the surface is dry enough and only some fluid patches remain at the corners of the unit cell in the (x,y) plane and at the bottom of the cavity (region VI); for even lower coverages, the finite configurations correspond to condensation at the bottom of the cavity. To illustrate the wetting and dewetting processes, some finite configurations corresponding to regions I–VI are shown in Fig. 9. Looking at the panels of the figure, the sequences I–II–III–IV and IV–V–VI–I, respectively, give a dynamical picture of the progress of wetting and of dewetting.

IV. RESULTS FOR Na SUBSTRATES

At variance with the case of Cs, the Na surface is known to be wetted by ^{4}He already at $T=0$. However, due to the relatively weak adsorption potential, its behavior is markedly different from most of other wettable surfaces, where one or two solid ^{4}He layers are formed on the substrate and are continuously wetted by the excess liquid. In weaker adsorbers such as Na, wetting is expected instead to occur preceded by a first-order prewetting transition. Quartz microbalance experiments confirm this scenario[52,55] and place an upper bound for the prewetting temperature at about 1–1.5 K. Theoretical calculations have shown that the prewetting transition is characterized by a two-layer jump in the coverage as the prewetting line is crossed.[31,56]

A. ^{4}He on planar Na

We computed first the isotherms μ vs Γ for homogeneous films on a flat Na surface, and afterward performed a Maxwell equal-area construction as described in Sec. III A. From each construction we get the value of the chemical potential below saturation where the jump from a thin to a thick film occurs, as expected in a first-order prewetting transition. We find that up to $T=2.7$ K such a construction is indeed possible. The next investigated value, $T=2.9$ K, appears to be already supercritical, thus placing our calculated T_{pw} around $T=2.8$ K. We show our computed prewetting line in Fig. 10. We find in particular that up to $T=1.6$ K the prewetting jump occurs from a thin film, which is just a tiny fraction of a monolayer, to a two-layer thick film, in agreement with

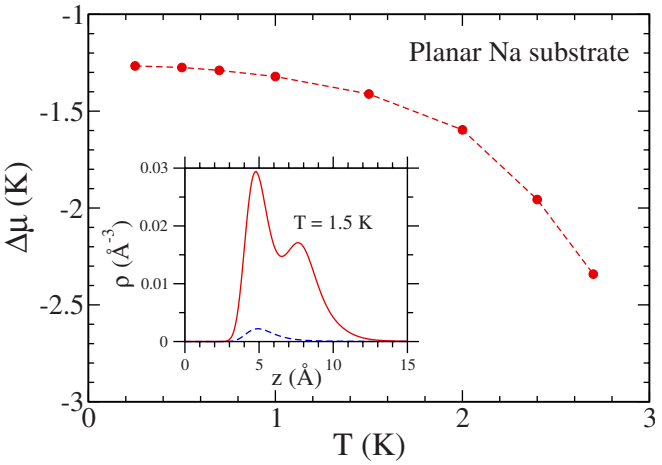

FIG. 10. (Color online) Calculated prewetting line $\Delta\mu$(K) as a function of T(K) for ^{4}He on an ideal planar Na surface. The dashed line is only a guide to the eye. The inset shows the density profiles of the thick film (solid line) and the thin film (dashed line) at T =1.5 K.

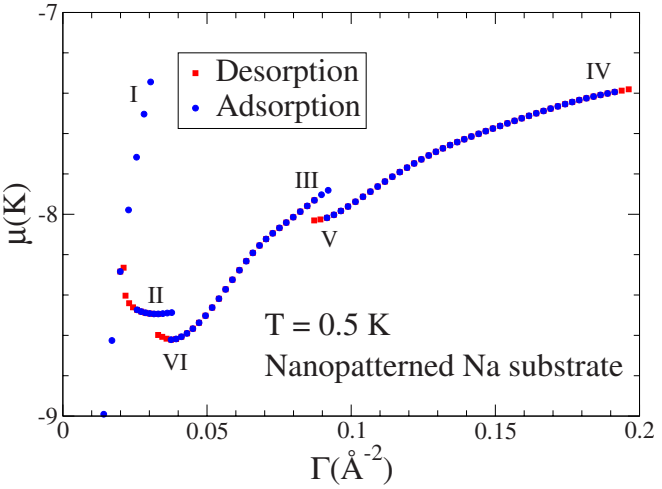

FIG. 11. (Color online) T=0.5 K isotherm for helium on the nanopatterned Na substrate. Circles (squares) represent finite configurations found in the adsorption (desorption) process. In regions II, III, and VI, some configurations in both processes have been found to be identical, and circles and squares overlap. The roman numerals I–VI indicate the regions where different type of finite configurations have been found in the calculation. Hysteretic loops are clearly visible.

previous theoretical predictions,[31,56] whereas at 2–2.4 K the jump is from the thin to a thick film corresponding roughly to one monolayer.

We summarize our findings in Fig. 10. The inset shows the thin and thick film density profiles at T=1.5 K. Our values for $\Delta\mu$ reported in Fig. 10 agree with the experimental results,[52] where the onset for growth of the adsorbed fluid on the microbalance is found to occur at $\Delta\mu \sim -1.4$ K for Na at T=1.6 K. Our estimated T_{pw} is, however, larger than the experimental value, where the onset of superfluidity for ^{4}He on Na via a Kosterlitz-Thouless (KT) transition occurs at about 1.6 K. In fact, since above such temperature the authors in Ref. 52 could not see any hysteretic loops in the isotherms, which are the hallmarks of any first-order transition, they deduce that T_{pw} should be lower than 1.6 K. The discrepancy between our results and the experimental findings could be due to various reasons. One possibility could be that the actual prewetting line for ^{4}He on Na meets the KT line just around 1.5–1.6 K, and terminates there; since we do not have the possibility to predict the KT transition in the FRDF frame, we actually see the prewetting line extending at higher temperature. A stronger motive is the fact that, being a mean-field theory, FRDF is not aimed at giving a good description of critical behavior, where long-range correlations play a key role. It has been shown[26,53] that temperature-dependent density functionals do overestimate the liquid-vapor critical temperature; moreover, a fluctuation theory that yields a complete classification of critical behavior, based on a Hamiltonian that accounts for highly anisotropic soft-mode fluctuations, demonstrates, i.e., that interfacial fluctuations have a strong influence on the character of the filling transition in a wedge.[54]

B. ^{4}He on nanostructured Na

We now address the changes in the wetting properties of a planar Na surface, as characterized in the previous section, due to the presence of a regular array of parabolic nanocavities. The substrate geometry is the same as described in Sec. II.

We have computed an isotherm at a relatively low temperature, T=0.5 K, and show the results in Fig. 11. To clarify the different portions of the isotherm, we have labeled them with roman numerals (cf. Fig. 8). The configurations found in the adsorption process are represented by circles, and those found in the desorption process are represented by squares. It can be seen that in some regions they sensibly coincide, e.g., most of region II, region IV above $\Gamma \sim 0.09$ Å^{-2}, and most of the portion of the isotherm labeled III and VI. Some relevant configurations belonging to regions I–VI are shown in Fig. 12.

We summarize our findings in the following: (i) the steep, rising part of the isotherm at low coverages (region I) corresponds to a continuous increase in ^{4}He within the parabolic cavity until it is completely filled with a slightly convex meniscus exactly at the level of the flat substrate, which is instead covered by a thin film (actually a tiny fraction of a monolayer, not visible with the resolution of Fig. 12). The highest coverage configuration we have found in this region is shown in the top left panel of Fig. 12; (ii) in the horizontal portion of the isotherm between $\Gamma \sim 0.025$ and ~ 0.04 Å^{-2} (region II), the parabolic cavity is not completely filled; the material inside has a concave meniscus below the level of the flat surface, as shown in the middle left panel of Fig. 12, and the amount of adsorbed fluid inside the cavity does not appreciably change in the whole range of coverages of branch II. What causes the actual change in coverage is the spreading of patches of liquid He, about two monolayers thick at the corners of the cell, i.e., in the flat region between the periodically repeated cavities, similarly to what happens during the growth of liquid He on a planar Na surface starting

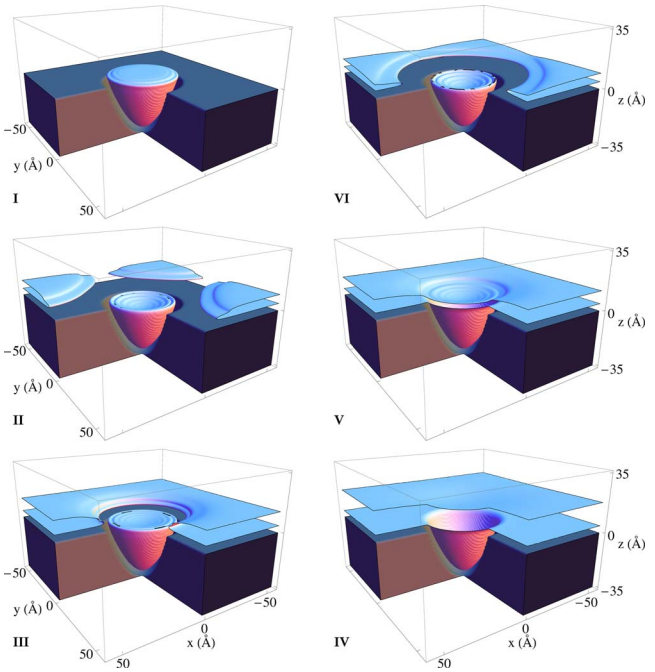

FIG. 12. (Color online) Counterclockwise, starting from the top left corner, the panels represent some illustrative equilibrium configurations for helium on the nanopatterned Na substrate corresponding to regions I–VI in Fig. 11. Chosen coverages: region I, $\Gamma=3.04\times10^{-2}$ Å^{-2}; region II, $\Gamma=3.78\times10^{-2}$ Å^{-2}; region III, $\Gamma=9.20\times10^{-2}$ Å^{-2}; region IV, $\Gamma=0.194$ Å^{-2}; region V, $\Gamma=8.93\times10^{-2}$ Å^{-2}; region VI, $\Gamma=3.59\times10^{-2}$ Å^{-2}. The panels display the isodensity surfaces for $\rho=0.011$ Å^{-3}, i.e., half the bulk liquid density at $T=0$ K. The dark area represents the Na planar surface. The stratification of the density due to the effect of the structured Na surface is clearly visible at the edge of finite configurations.

from finite patches, as found in Ref. 31. Note that, in the substrate domains not yet invaded by such patches, there is only a thin submonolayer film, whose width remains constant in the whole region II; (iii) in the concave short portion of the isotherm around $\Gamma=0.04$ Å^{-2} (region VI), the liquid patches on the flat surface have merged together and only the heliophobic ring-shaped region around the edge of the cavity remains covered by a thin film while the cavity itself becomes completely filled with a slightly concave meniscus at the level of the flat substrate, as seen in the top right panel of Fig. 12; (iv) the hysteretic loop at coverages around $\Gamma=0.09$ Å^{-2} (regions III and V) is related to the filling/emptying of the annular region around the edge of the cavity: this is left almost void of fluid as the corner droplets have merged on the flat surface when the coverage is increased (upper branch III), whereas it is wetted by He when the coverage is decreased (lower branch V). The two corresponding density configurations are shown in the bottom left and middle right panels, respectively, of Fig. 12. (v) At relatively higher coverages (region IV) a very thick film made of several monolayers covers everything, including the filled parabolic cavities, and grows continuously with increasing μ. This is plotted in the bottom right panel of Fig. 12.

We mention that, in Ref. 57, it has been shown that, in a parabolic cavity, a meniscus does not appear until the chemical potential exceeds a certain threshold. This is not the case in the current calculations where a meniscus appears for all coverages and associated values of the chemical potential, as illustrated in Fig. 13, where we show the density contours for helium in a Cs (top panel) and a Na (bottom panel) cavity for a coverage $\Gamma=0.004$ Å^{-1} at a temperature of 0.5 K. To our understanding, this is due to finite-size effects that can reveal the sensitivity of the nanoscopic samples to the details of the adsorption potential, whereas the model of Ref. 57 is exact in the macroscopic limit and is not intended to be a microscopic description of the phenomena involved. Moreover, the substrates considered here are "weak" adsorbers: the filling of a parabolic cavity on a stronger substrate might proceed in a very different way, e.g., similarly to what is described in Ref. 57.

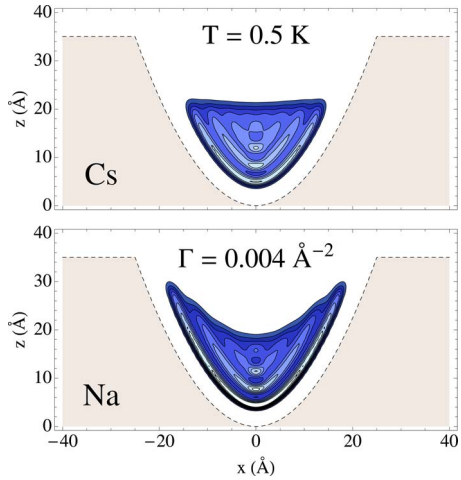

FIG. 13. (Color online) Density contours of helium in Cs and Na parabolic cavities at a very low coverage to illustrate the appearance of a concave meniscus. The darker the region, the lower the helium density.

V. SUMMARY AND OUTLOOK

In this work we have computed the isotherms of the ^{4}He-Cs system, and their modifications in the presence of a Cs surface structured with a lattice of parabolic nanocavities. Employing a largely tested T-dependent FRDF, we have performed a theoretical construction of the prewetting line of ^{4}He on homogeneous semi-infinite Cs, up to 3 K. To the best of our knowledge, this has not been carried out before. The wetting temperature is in good agreement with previous theoretical and experimental determinations while the prewetting one seems to be higher than that indicated by the experiments.[13] Restrictions in the parametrization of the FRDF prevent us from reaching temperatures higher than 3 K in our calculations. We have shown that the ability to nucleate finite superficial configurations such as drops and bubbles—respectively, patches of the thick and of the thin film—is the key to remove the mechanically unstable region in the adsorption isotherms, however giving rise to hysteretic cycles. As the flat homogeneous substrate is patterned with nanocavities, finite systems such as drops and bubbles are natural competitors to homogeneous layers on the surface,

and provoke visible modifications of the isotherms. We compare the He-Cs and He-Na systems, for either flat and structured substrates, and find rather similar qualitative characteristics in the wetting and filling patterns, in spite of the nonwettability of Cs that contrasts with Na wettability at zero temperature, as reflected by the computed prewetting lines.

The coexistence of a thin and a thick helium film on a wetted surface along the prewetting line may deserve further research although no observation of this coexistence in any He alkali has been reported. It has been predicted that the line tension diverges logarithmically in systems with nonretarded van der Waals forces as the wetting transition is approached.[58] As a consequence, it has been shown that, on a simple capillary approximation,[59] the barrier for nucleation of thin patches (bubbles) in the thick film diverges in the vicinity of the wetting temperature. Several authors[3,4,13,40,60] have pointed out that a metastable thick film of helium on Cs has an exceedingly long lifetime and can persist, upon cooling, for temperatures below T_w while a thin metastable film could be extremely short lived to be experimentally observed. More recently, the nonwetting thin-film state of ^{4}He on Cs was investigated using the photoelectron tunneling technique,[61] and it was possible to observe the growth of a submonolayer film for very unsaturated vapor pressure conditions. This growth stops, and very close to liquid-vapor coexistence, the adsorbed helium layer is increased to a liquidlike phase a few monolayers wide, with Cs remaining in the nonwet state. We believe that a determination of thin-film–thick-film coexistence above the wetting temperature could shed light on the mechanisms of drop and bubble nucleations in the neighborhood of a wall.

Finally, a tentative by-product of our capacity to evaluate density profiles together with thermodynamic parameters of the helium samples is the possibility of examining, in the near future, the appearance and structure of helium rings surrounding nanocavities or nanohills of arbitrary shape, which could be particularly interesting in view of the predicted existence of ^{3}He edge states in finite configurations of isotopic helium mixtures.[62]

ACKNOWLEDGMENTS

We are pleased to acknowledge fruitful discussions with Ignacio Pagonabarraga, and useful exchanges with Adrian Wyatt and Milton Cole. This work has been performed under Grant No. FIS2008-00421/FIS from DGI, Spain (FEDER), Grant No. 2005SGR00343 from Generalitat de Catalunya and in Argentina, Grant No. PIP 5138/05 from CONICET, and Grant No. PICT 31980/05 from ANPCYT. F.A. acknowledges the support of Padova University through Project No. CPDA077281-07, and A.H. has been funded by the Project HPC-EUROPA (Project No. RII3-CT-2003-506079), with the support of the European Community - Research Infrastructure Action under the FP6 "Structuring the European Research Area" Programme.

[1] J. W. Cahn, J. Chem. Phys. **66**, 3667 (1977).
[2] C. Ebner and W. F. Saam, Phys. Rev. Lett. **38**, 1486 (1977).
[3] D. Bonn and D. Ross, Rep. Prog. Phys. **64**, 1085 (2001).
[4] B. M. Law, Prog. Surf. Sci. **66**, 159 (2001).
[5] E. Cheng, M. W. Cole, W. F. Saam, and J. Treiner, Phys. Rev. Lett. **67**, 1007 (1991); E. Cheng, M. W. Cole, W. F. Saam, and J. Treiner, Phys. Rev. B **46**, 13967 (1992); E. Cheng, M. W. Cole, J. Dupont-Roc, W. F. Saam, and J. Treiner, Rev. Mod. Phys. **65**, 557 (1993).
[6] P. Taborek and J. E. Rutledge, Phys. Rev. Lett. **68**, 2184 (1992).
[7] P. Taborek and J. E. Rutledge, Phys. Rev. Lett. **71**, 263 (1993).
[8] D. Ross, P. Taborek, and J. E. Rutledge, J. Low Temp. Phys. **111**, 1 (1998).
[9] E. Rolley and C. Guthmann, J. Low Temp. Phys. **108**, 1 (1997).
[10] J. Dupont-Roc and X. Müller, Physica B **284-288**, 143 (2000); X. Müller, T. Kinoshita, and J. Dupont-Roc, J. Low Temp. Phys. **113**, 823 (1998); A. Prevost, E. Rolley, and C. Guthmann, Phys. Rev. B **65**, 064517 (2002); A. F. G. Wyatt and J. Klier, Phys. Rev. Lett. **85**, 2769 (2000).
[11] J. Klier, P. Leiderer, D. Reinelt, and A. F. G. Wyatt, Phys. Rev. B **72**, 245410 (2005).
[12] A. Prevost, E. Rolley, and C. Guthmann, Phys. Rev. Lett. **83**, 348 (1999).
[13] J. E. Rutledge and P. Taborek, Phys. Rev. Lett. **69**, 937 (1992).
[14] A. Chizmeshya, M. W. Cole, and E. Zaremba, J. Low Temp. Phys. **110**, 677 (1998).
[15] E. Robens, P. Staszczuk, A. Dabrowski, and M. Barczak, J. Therm. Anal. Calorim. **79**, 499 (2005).
[16] L. D. Gelb, K. E. Gubbins, R. Radhandakrishnan, and M. Sliwinska-Bartkowiak, Rep. Prog. Phys. **62**, 1573 (1999).
[17] A. Neimark, P. I. Ravikovich, and A. Vishnaykov, J. Phys.: Condens. Matter **15**, 347 (2003).
[18] L. Bruschi, G. Fois, G. Mistura, M. Tormen, V. Garbin, E. di Fabrizio, A. Gerardino, and M. Natali, J. Chem. Phys. **125**, 144709 (2006).
[19] V. Apaja and E. Krotscheck, Phys. Rev. B **67**, 184304 (2003); Phys. Rev. Lett. **91**, 225302 (2003).
[20] M. Rossi, D. E. Galli, and L. Reatto, Phys. Rev. B **72**, 064516 (2005); M. Rossi, D. E. Galli, and L. Reatto, J. Low Temp. Phys. **146**, 95 (2007).
[21] M. W. Cole, F. Ancilotto, and S. M. Garcia, J. Low Temp. Phys. **138**, 195 (2005).
[22] A. Hernando, E. S. Hernández, R. Mayol, and M. Pi, Phys. Rev. B **77**, 195431 (2008).
[23] F. Ancilotto, A. M. Sartori, and F. Toigo, Phys. Rev. B **58**, 5085 (1998).
[24] E. S. Hernández, F. Ancilotto, M. Barranco, R. Mayol, and M. Pi, Phys. Rev. B **73**, 245406 (2006).
[25] F. Ancilotto, F. Faccin, and F. Toigo, Phys. Rev. B **62**, 17035 (2000).
[26] A. Guirao, M. Centelles, M. Barranco, M. Pi, A. Polls, and X. Viñas, J. Phys.: Condens. Matter **4**, 667 (1992).
[27] O. Gang, K. J. Alvine, M. Fukuto, P. S. Pershan, C. T. Black, and B. M. Ocko, Phys. Rev. Lett. **95**, 217801 (2005); O. Gang, K. J.

Alvine, M. Fukuto, P. S. Pershan, C. T. Black, and B. M. Ocko *ibid.* **98**, 209904(E) (2007).
[28] N. D. Mermin, Phys. Rev. **137**, A1441 (1965).
[29] E. S. Hernández, F. Ancilotto, M. Barranco, R. Mayol, and M. Pi, Phys. Rev. B **73**, 245406 (2006).
[30] M. Barranco, R. Guardiola, S. Hernández, R. Mayol, J. Navarro, and M. Pi, J. Low Temp. Phys. **142**, 1 (2006).
[31] M. Barranco, M. Guilleumas, E. S. Hernández, R. Mayol, M. Pi, and L. Szybisz, Phys. Rev. B **68**, 024515 (2003).
[32] W. H. Press, S. A. Teulosky, W. T. Vetterling, and B. P. Flannery, *Numerical Recipes in Fortran 77: The Art of Scientific Computing* (Cambridge University Press, Cambridge, 1999).
[33] M. Frigo and S. G. Johnson, Proc. IEEE **93**, 216 (2005).
[34] A. Hernando, E. S. Hernández, R. Mayol, and M. Pi, Phys. Rev. B **76**, 115429 (2007).
[35] A. Neimark and A. Vishnyakov, J. Chem. Phys. **122**, 054707 (2005).
[36] A. V. Neimark and A. Vishnyakov, Phys. Rev. E **62**, 4611 (2000).
[37] V. Iov, J. Klier, and P. Leiderer, Physica B **329-333**, 242 (2003).
[38] T. McMillan, J. E. Rutledge, and P. Taborek, J. Low Temp. Phys. **138**, 995 (2005).
[39] M. Zech, H. Bromberger, J. Klier, P. Leiderer, and A. F. G. Wyatt, Phys. Rev. B **78**, 115113 (2008).
[40] R. Bausch and R. Blossey, Phys. Rev. E **48**, 1131 (1993).
[41] F. B. Wyart and J. Daillant, Can. J. Phys. **68**, 1084 (1990).
[42] M. Elbaum and S. G. Lipson, Phys. Rev. Lett. **72**, 3562 (1994).
[43] L. M. Pismen, Phys. Rev. E **70**, 021601 (2004).
[44] M. Barranco, M. Guilleumas, M. Pi, and D. M. Jezek, in *Microscopic Approaches to Quantum Liquids in Confined Geometries*, edited E. Krotscheck and J. Navarro, Series on Advances in Quantum Many-Body Theory (World Scientific, Singapore, 2002), Vol. 4, p. 319.
[45] S. Balibar, J. Low Temp. Phys. **129**, 363 (2002).
[46] M. Lassaut, H. Flocard, P. Bonche, P. H. Heenen, and E. Suraud, Astron. Astrophys. **183**, L3 (1987).
[47] A. Sharma and R. Khanna, Phys. Rev. Lett. **81**, 3463 (1998).
[48] E. Cheng and J. Treiner, J. Low Temp. Phys. **101**, 331 (1995).
[49] V. E. Smorodin, Langmuir **10**, 2250 (1994).
[50] K. Kargupta, R. Konnur, and A. Sharma, Langmuir **16**, 10243 (2000); **17**, 1294 (2001).
[51] S. Curtarolo, G. Stan, M. W. Cole, M. J. Bojan, and W. A. Steele, Phys. Rev. E **59**, 4402 (1999).
[52] J. A. Phillips, P. Taborek, and J. E. Rutledge, J. Low Temp. Phys. **113**, 829 (1998).
[53] T. Biben and D. Frenkel, J. Phys.: Condens. Matter **14**, 9077 (2002).
[54] A. O. Parry, C. Rascón, and A. J. Wood, Phys. Rev. Lett. **85**, 345 (2000).
[55] G. Mistura and M. H. W. Chan, Physica B **284-288**, 135 (2000).
[56] M. Boninsegni and L. Szybisz, Phys. Rev. B **70**, 024512 (2004).
[57] C. Rascón and A. O. Parry, Nature (London) **407**, 986 (2000).
[58] J. O. Indekeu, Physica A **183**, 439 (1992).
[59] M. Schick and P. Taborek, Phys. Rev. B **46**, 7312 (1992).
[60] D. Bonn, H. Kellay, and J. Meunier, Phys. Rev. Lett. **73**, 3560 (1994).
[61] D. Reinelt, V. Iov, P. Leiderer, and J. Klier, J. Phys.: Condens. Matter **17**, S403 (2005).
[62] R. Mayol, M. Barranco, E. S. Hernández, M. Pi, and M. Guilleumas, Phys. Rev. Lett. **90**, 185301 (2003).